Carbon nanotube Q-switched Yb:KLuW surface channel waveguide lasers

Ji Eun Bae,[1] Tae Gwan Park,[1] Esrom Kifle,[2] Xavier Mateos,[2] Magdalena Aguiló,[2] Francesc Díaz,[2] Carolina Romero,[3] Javier Rodríguez Vázquez de Aldana,[3] Hansuek Lee,[1,4] and Fabian Rotermund[1,*]

[1]Department of Physics, Korea Advanced Institute of Science and Technology (KAIST), 34141 Daejeon, Korea
[2]Física i Cristal·lografia de Materials I Nanomaterials (FiCMA-FiCNA), Universitat Rovira i Virgili (URV), E-43007 Tarragona, Spain
[3]Aplicaciones del Láser y Fotónica, University of Salamanca, 37008 Salamanca, Spain
[4]Graduate School of Nanoscience and Technology, Korea Advanced Institute of Science and Technology (KAIST), 34141 Daejeon, Korea
*Corresponding author: rotermund@kaist.ac.kr

Received XX Month XXXX; revised XX Month, XXXX; accepted XX Month XXXX; posted XX Month XXXX (Doc. ID XXXXX); published XX Month XXXX

A channel waveguide buried immediately below the surface of a Yb:KLuW crystal is used as a laser gain medium for passive Q-switching by both evanescent- and direct-field interactions with single-walled carbon nanotubes (SWCNTs) near 1040 nm. The SWCNTs used as saturable absorbers (SAs) are deposited on top of the half-ring-type channel waveguide fabricated via femtosecond direct laser writing. The Q-switched waveguide laser delivers 88.5-ns pulses at a 1.16-MHz repetition rate with a maximum average output power of 680 mW. For the two different interaction schemes with SWCNT-SAs, the pulse characteristics depending on the output coupling ratio and absorbed pump power are experimentally investigated and compared to the results of theoretical analysis of the SA Q-switched operation.

OCIS codes: *(140.3540) Lasers, Q-switched; (230.7380) Waveguides, channeled; (140.3380) Laser materials; (190.4400) Nonlinear optics, materials.*

http://dx.doi.org/10.1364/OL.99.099999

Efficient pulsed lasers in compact cavity designs provide considerable potential for practical applications including metrology, spectroscopy, and microscopy [1-5]. In particular, chip-size optical elements and coherent sources can be usefully applied to integrated photonics. For the 1-μm spectral region, ytterbium ions (Yb^{3+}) have been actively used as an active dopant because of their potential for realizing diode-pumped high-power lasers and ultrashort pulse generation in mode-locked lasers. Unlike glass-based gain media, Yb-doped crystals or ceramic materials, particularly Yb-doped monoclinic double tungstate crystals such as $KLu(WO_4)_2$ (KLuW), $KGd(WO_4)_2$ and $KY(WO_4)_2$, show excellent mechanical and thermal properties, broad and relatively high absorption/emission cross-sections, and extremely low quantum defects that make them beneficial for utilization in efficient lasers.

Recently, waveguide (WG) structures have emerged as a great candidate for miniaturizing lasers because of their well-confined guiding properties. They support high intracavity pump intensities with excellent overlap between the pump and laser modes owing to efficient confinement of the fundamental mode, and consequently lead to low lasing thresholds and high efficiencies. To fabricate channel WGs in transparent materials, the femtosecond direct laser writing (fs-DLW) technique was recently suggested as among the most reliable techniques [6, 7]. Such channel WGs allow delivery of a circular single-mode output after propagating the entire length of the WGs, enabling efficient laser operation.

Passive Q-switching utilizing a saturable absorber (SA) is a well-established method for generating nanosecond pulses in solid-state lasers. Low-dimensional materials including graphene [8], carbon nanotubes (CNTs), topological insulators [9] and transition metal dichalcogenides (TMDs) [10] have recently become promising SAs for miniaturized ultra-compact lasers [11, 12]. They can be used for efficient pulsed operation based on direct- and evanescent-field interaction and allow monolithic integration in the cavity, while semiconductor saturable absorber mirrors and crystal-based SAs are mostly integrated between the laser gain medium and mirrors [13-15]. Regarding nanocarbons, single-walled carbon nanotubes (SWCNTs) and graphene show unique linear and nonlinear optical properties including an intrinsic ultrafast response, large third-order nonlinearity, broadband nonlinear absorption, and flexible applicability for integration. The relatively simple, cost-effective, and controllable fabrication process of such SAs provides additional advantages for diverse forms of compact pulsed lasers.

Compact cavity designs utilizing Yb-doped gain materials have been recently demonstrated in various configurations. Based on a bulk crystal without WG structures, solid-state microchip lasers have been studied because of their low losses and insensitivity to alignment, enabling higher laser efficiency and output power. The Q-switched Yb-doped microchip lasers have been demonstrated using Cr:YAG, TMDs and graphene placed between the microchip

and the output coupler (OC) only based on direct-field (reflective/transmissive) coupling [15-18].

Yb-doped planar and channel WGs as gain media have also been investigated for the pulsed laser operation near 1 μm [12, 13, 19-22]. For the evanescent-field interaction, Yb-doped planar WG lasers are Q-switched using graphene and SWCNTs [12, 19-21]. The reported results are limited to only planar WGs. However, the channel WG structures have the potential for improved laser efficiency, stability, and circular single-mode operation compared to that of planar WGs. Here, we report diode-pumped SWCNT-Q-switched Yb:KLuW channel WG lasers based on direct- and evanescent-field interaction. To the best of our knowledge, this is the first demonstration of Q-switched Yb-doped channel WG lasers based on interaction between SWCNTs and the evanescent field. SWCNTs are deposited on the top surface of the channel WG for evanescent-field coupling and the OCs for a reflective type. The Q-switched laser cavity consists of two different light interaction types using a Yb:KLuW WG and laser mirrors (a highly reflective incoupling mirror and the OCs) that are attached parallel to both end-facets of the WG. The Q-switched operation characteristics with different OC ratios and pump powers are investigated. Subsequently, the experimental results are compared to the theoretically analyzed results for a SA Q-switched laser operation.

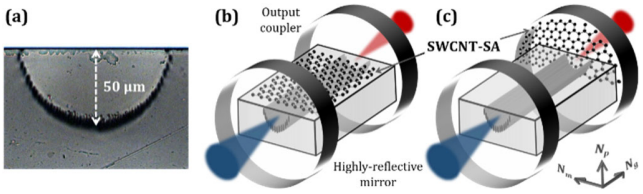

Fig. 1. (a) Optical microscope image of the surface-buried channel WG with a vertical width of 50 μm and a schematic of the Q-switched Yb:KLuW channel WG lasers based on (b) evanescent- and (c) direct-field interaction with SWCNT-SA.

Depressed-index surface channel WGs were fabricated in a bulk 5 at.% Yb^{3+}-doped KLuW crystal via fs-DLW. The active crystal was grown using the Top-Seeded-Solution Growth (TSSG) Slow-Cooling method with $K_2W_2O_7$ as a solvent and a [010]-oriented seed [23]. Yb:KLuW is monoclinic (sp. gr. C^6_{2h} – C2/c) and optically biaxial. The crystal was oriented along the N_g axis of the optical indicatrix because it provides access to the high-gain $E \parallel N_m$ polarization. The sample length was 2.88 mm. Its aperture was 2.93 (N_m) × 3.05 (N_p) mm^2 and both $N_m \times N_p$ faces were polished to laser-grade quality and remained uncoated. For the inscription, a Ti:sapphire regenerative amplifier emitting 120-fs pulses at 795 nm at a repetition rate of 1 kHz was used. The laser beam was focused on the crystal using a 40× microscope objective (N.A. = 0.65). The incident pulse energy was adjusted to 65 nJ after the focusing optics. The crystal was scanned at 400 μm/s along its N_g axis producing damage tracks. The WG consisted of a semicircular undamaged core surrounded by a half-ring of damage tracks with a radius of 50 μm. The optical microscope image of the WG is shown in Fig. 1(a). The lateral separation between adjacent tracks was 2 μm.

The basic material used for the fabrication of SAs is arc-discharged SWCNTs (Meijo Nano Carbon Co., Ltd). The SWCNT powders, which show broadband absorption within the 1-μm spectral range which corresponds to the E_{22} interband transitions of SWCNTs, are dissolved in 1,2-dichlorobenzene (o-DCB) with surfactant at desired concentrations. They are agitated in an ultrasonic bath. To remove bundles and impurities, the solution is centrifuged for about 20 min. The well-dispersed SWCNT solution is then mixed with a separately prepared polymethyl methacrylate (PMMA) (Polymer Source, Inc.) solution (100 mg/mL in o-DCB).

For evanescent-field interaction with the guided beam, the SWCNT/PMMA composite solution with a SWCNT concentration of 0.5 mg/mL is spin-coated on the top surface of the Yb:KLuW crystal containing a surface channel WG. The entire area of the top surface is coated. The front and end facet of the WG are protected during the deposition and finally cleaned. In addition, all OCs used in this work to study the direct-field interaction with laser beams are spin-coated under the same condition using the solution with a SWCNT concentration of 0.15 mg/mL. The nonlinear optical characteristics are investigated at 1030 nm using SWCNT-coated 1-mm-thick fused silica quartz. The SWCNT-SA shows a modulation depth of 0.11% and nonsaturable losses of 0.79% with a saturation fluence of 49 $\mu J/cm^2$. The measured time-resolved pump-probe response can be fitted via a bi-exponential function, delivering a fast component of 251 fs and a slow decay of 1.9 ps.

The Q-switched WG laser setups with two different interaction schemes employing the SWCNT-SA are shown in Fig. 1(b) and (c). A tapered amplifier diode laser system (TA pro, Toptica Photonics, Inc.) operating at 981.6 nm is used as a pump source. The pump beam passes through a half-wave plate, a polarizer, and a half-wave plate to control the incident pump power and polarization. The linearly polarized ($E \parallel N_m$) pump beam is then focused on the WG front facet using a plano-convex lens through an incoupling mirror. This mirror simultaneously serving as the end mirror is highly transparent at the pump wavelength and highly reflective at the laser wavelength. The Yb:KLuW crystal containing the surface channel WG is mounted on the multi-axis stage without additional cooling. An OC is attached to the other end facet of the WG. The output laser beam is then analyzed after passing through a long-pass filter for filtering out the residual pump beam.

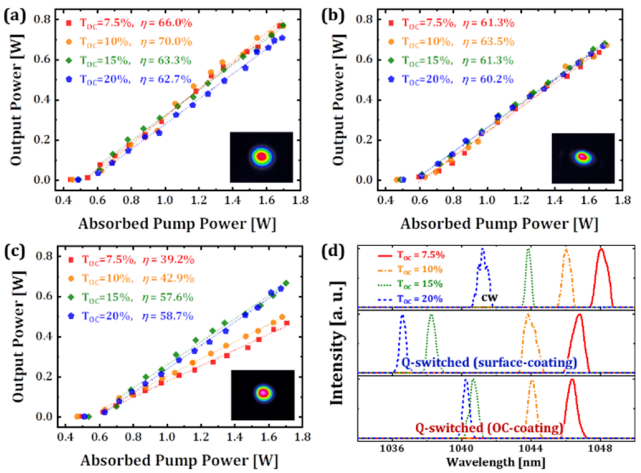

Fig. 2. Measured input-output power dependences in (a) cw and Q-switched operation based on (b) evanescent- and (c) direct-field interaction (inset: beam profiles at a maximum power with T_{OC}=15%). (d) Laser emission spectra measured in cw (top), Q-switched operation based on evanescent- (middle) and direct-field interaction (bottom).

We first measured the continuous-wave (cw) performance without integration of the SWCNT-SAs. Achieved output powers versus absorbed pump powers with different OC ratios of T_{OC}=7.5,

10, 15, and 20% are shown in Fig. 2(a) with the measured beam profile at maximum output power for T_{OC}=15% (inset). The absorbed pump power is estimated by considering the Fresnel losses at the WG facets and the absorption under the lasing condition. The laser emission begins from an absorbed pump power of less than ~491 mW in all cases. The lasing threshold is reduced with decreasing T_{OC} which provides a higher intracavity energy. The slope efficiencies are shown to be 66%, 70%, 63%, and 63% for T_{OC}=7.5, 10, 15, and 20%, respectively. The maximum cw output power amounted to 770 mW with T_{OC}=15% at a 1.7-W absorbed pump power. The propagation loss within the WG was estimated from a modified Caird analysis for the cw mode from T_{OC}=1 to 20% [24]. The resultant propagation loss amounts to 0.61 ± 0.11 dB/cm. This result indicates a high-quality channel WG leading to efficient operation of the surface channel WG lasers.

Q-switched operation of the Yb:KLuW channel WG laser is achieved using SWCNT-SAs spin-coated on top of the surface WG or on the OC. No special alignment is required for achieving the Q-switched operation. The measured input-output dependences for each case are plotted in Fig. 2(b) and (c). For Q-switching via the evanescent-field interaction, a maximum output power of 680 mW is generated with η= 61% at an OC ratio of 15%. Considering the output power observed in the cw performance, the Q-switching conversion from the cw operation is 90.7%. The very high ratio reflects a low SA insertion loss, which leads to a highly efficient Q-switched operation. However, Q-switching via direct-field interaction provides a maximum power of 666 mW with η = 58% at an OC ratio of 15%, and the Q-switching conversion is 86.2%. The measured Q-switched beam profiles at the maximum pump powers are shown in the inset of Fig. 2(b) and (c), and show well-defined fundamental modes in both cases. The stable Q-switched operation results in a pulse-to-pulse intensity fluctuation of < 10%, as shown in Fig. 3(a) and (b). The recorded laser spectra of each interaction type are shown in Fig. 2(d). Because of the broadband gain of the Yb:KLuW crystal, the spectra can be tuned near 1040 nm. A blue shift of the laser wavelength with higher OC ratios is observed. This result is mainly attributed to increased cavity losses inducing a larger gain cross-section to compensate for the losses, thus increasing the inversion ratio [23]. Note that the polarization states of both cw and Q-switched lasers are the same as that of the pump polarization $E \parallel N_m$.

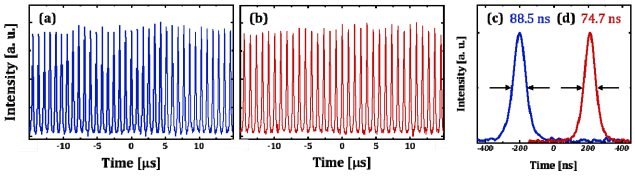

Fig. 3. Q-switched pulse train and the shortest pulse measured at the maximum output power with T_{OC}=15% for (a), (c) evanescent- and (b), (d) direct-field interaction.

The Q-switched pulse characteristics for both evanescent- and direct-field interaction schemes are measured depending on the absorbed pump power. The pulse repetition rate (f_{rep}) and pulse duration (full-width at half-maximum (FWHM)), $\Delta\tau_p$) are directly obtained from the oscilloscope trace (1-GHz Tektronix, TDS784D) using a fast InGaAs photodiode. The peak power P_{peak} is calculated from the measured values as $P_{peak} = P_{out}/(f_{rep} \cdot \Delta\tau_p)$. The results are obtained with all OCs; the case of T_{OC}=15% is summarized in Fig. 4.

For the direct-field interaction with the SWCNT-SA, the pulse duration decreases from 143 to 74.7 ns with increasing pump power when the repetition rate is increased from 0.758 to 1.09 MHz. The Q-switched pulse train and pulse width at the maximum absorbed pump power are shown in Fig. 3(b) and (d). Consequently, the maximum peak power of 8.21 W and the corresponding pulse energy of 613 nJ are obtained at the maximum pump power of 1.7 W. Subsequently, the experimental results are compared to the results from theoretical analysis. Note that the theoretical modeling of the Q-switched operation is based on the numerical solution of the rate equations for a quasi-three-level gain medium and a fast SA having fluence-dependent nonlinear absorption [14, 16, 25].

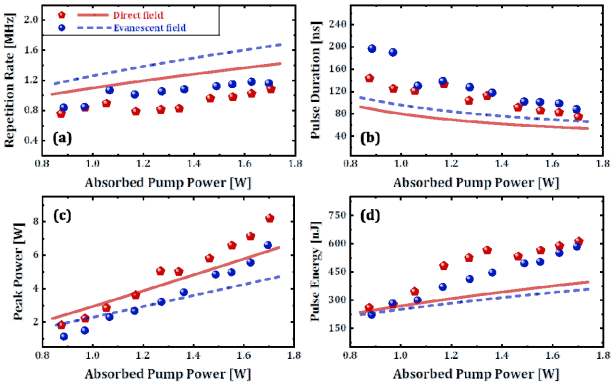

Fig. 4. Q-switched laser properties with T_{OC}=15% for two interaction types: (a) pulse repetition rate, (b) pulse duration, (c) pulse peak power, and (d) pulse energy (Dots: experiments, Lines: modeling).

The results of the pump-power-dependent theoretical analysis are also plotted in Fig. 4 as solid lines for the direct-field interaction. For theoretical modeling, the nonlinear absorption parameters of the SWCNT-SA measured in a SWCNT-coated 1-mm-thick fused silica quartz at 1030 nm are used. The tendency and value of the pulse characteristics achieved during the experiment are fairly comparable to the theoretical results. However, the acceptable discrepancy might have additionally originated from practical issues including insufficient absorption of the pump power in the WG and additional losses including scattering loss from the SAs as well as the WG. In addition, the higher values in peak power and pulse energy achieved in the experiment compared to the theoretical modeling are attributed to the confined geometry of our channel WG structure that results in more efficient laser operation.

For the indirect interaction of the evanescent field, the shortest pulse duration achieved is 88.5 ns at a maximum pump power for T_{OC}=15%, accompanying an increase in the repetition rate from 0.84 to 1.16 MHz as shown in Fig. 3(a) and (c). The maximum peak power is 6.61 W and the corresponding pulse energy is 585 nJ. For evanescent-field interaction, it is generally not a trivial task to experimentally estimate the exact nonlinear absorption properties of the surface-coated SA including the interaction peak intensity and modulation depth. Thus, we built a qualitative model based on weaker nonlinear absorption and nonsaturable loss than in the case of direct-field interaction, owing to the longer pulse duration and lower SA-insertion loss experimentally achieved as shown in Fig. 4.

In the constructed model assuming a modulation depth of 0.01% and a nonsaturable loss of 0.25%, the pulse characteristics tend to be quite similar to the experimental results for the evanescent-field case. From this result, we can expect that the evanescent-field interaction shows a modulation of approximately 0.01% for the entire propagation of the WG which is sufficient for stable Q-switched operation.

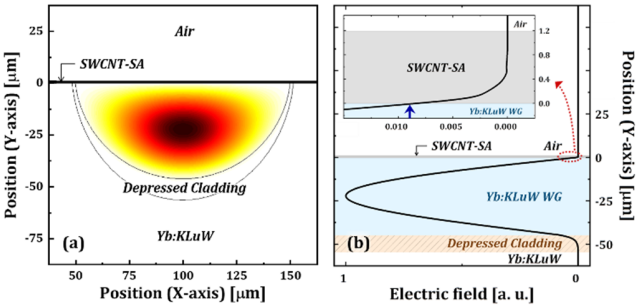

Fig. 5. (a) Calculated electric field distribution on the SWCNT SA-coated Yb:KLuW surface channel WG and (b) its side-view of the vertical cross-section at the electric field maximum.

The fundamental laser mode confinement within the channel WG is verified by the calculated electric field distribution as shown in Fig. 5(a). The WG dimension is estimated from the optical microscope image (Fig. 1) and the SWCNT-SA layer thickness is 1.2 μm. Figure 5(b) shows a side view of the vertical cross-section at the maximum of the normalized electric field distribution in the Yb:KLuW channel WG and SWCNT-SA. The magnitude of the electric field in the SWCNT-SA is approximately 0.009% of that in the Yb:KLuW channel (inset of Fig. 5(b)). The extracted field traveling through the WG leads to a stable Q-switched operation with an extremely low Q-switching conversion loss.

In conclusion, the Yb:KLuW surface channel WG fabricated via fs-DLW is passively Q-switched by both surface- and OC-coated SWCNT-SAs. The Q-switched operation using the evanescent-field is demonstrated in Yb-doped channel WG lasers for the first time. The Q-switched WG lasers are advantageous when compared to Yb-fiber lasers Q-switched by evanescent-field coupling with SAs. The fiber lasers typically possess large nonsaturable losses and long cavity length of more than 1 m [26, 27]. Furthermore, the channel WG lasers demonstrated in this work show highly efficient Q-switched operation and a lower lasing threshold compared to that of Yb:KLuW microchip lasers [15-18]. We can also compare our Q-switched lasers with Yb-doped planar-like WG lasers Q-switched by evanescent-field interaction. Our approach provides well-defined symmetric beam modes, higher output powers and slope efficiencies in a simplified cavity design [12, 19-21]. In our case of evanescent-field coupling, 88.5-ns pulses at a 1.16-MHz repetition rate with a maximum output power of 680 mW are generated from a 2.88-mm-long cavity with T_{OC}=15%. The process provides a high Q-switching conversion from the cw operation with a very low SA insertion loss. For the direct-field interaction with OC-coated SWCNT-SA, 74.7-ns pulses are achieved at a repetition rate of 1.09 MHz with a maximum output power of 666 mW. For both types of interaction, the characteristics of Q-switched pulses could be further controlled by varying the SA parameters. The experimental results compared to the theoretical results analyzed for passive Q-switching with a fast SA provide reasonable agreement for the pulsed characteristics. Our approaches can be further optimized to realize a monolithic design of compact pulsed lasers.

Funding. National Research Foundation of Korea (NRF) (2017R1A4A1015426, 2018H1A2A1061480), Spanish Government (MAT2016-75716-C2-1-R (AEI/FEDER,UE), FIS2017-87970-R); Junta de Castilla y León (SA287P18); Generalitat de Catalunya (2017SGR755).

References

1. T. M. Fortier, A. Bartels, and S. A. Diddams, Opt. Lett. **31**, 1011 (2006).
2. Y. N. Billeh, M. Liu, and T. Buma, Opt. Express **18**, 18519 (2010).
3. R. Aviles-Espinosa, G. Filippidis, C. Hamilton, G. Malcolm, K. J. Weingarten, T. Südmeyer, Y. Barbarin, U. Keller, S. I.C.O Santos, D. Artigas, and P. Loza-Alvarez, Biomed. Opt. Express **2**, 739 (2011).
4. M. P. Moreno and S. S. Vianna, J. Opt. Soc. Am. B **28**, 2066 (2011).
5. S. Pekarek, T. Südmeyer, S. Lecomte, S. Kundermann, J. M. Dudley, and U. Keller, Opt. Express **19**, 16491 (2011).
6. R. R. Gattass and E. Mazur, Nat. Photonics **2**, 219 (2008).
7. F. Chen and J. R. V. de Aldana, Laser Photonics Rev. **8**, 251 (2014).
8. H. Yu, X. Chen, H. Zhang, X. Xu, X. Hu, Z. Wang, J. Wang, S. Zhuang, and M. Jiang, ACS Nano **4**, 7582 (2010).
9. H. Yu, H. Zhang, Y. Wang, C. Zhao, B. Wang, S. Wen, H. Zhang, and J. Wang, Laser Photon. Rev. **7**, L77 (2013).
10. S. Wang, H. Yu, H. Zhang, A. Wang, M. Zhao, Y. Chen, L. Mei, and J. Wang, Adv. Mater. **26**, 3538 (2014).
11. Z. Li, Y. X. Zhang, C. Cheng, H. H. Yu, and F. Chen, Opt. Express **26**, 11321 (2018).
12. J. W. Kim, S. Y. Choi, J. E. Bae, M. H. Kim, Y. U. Jeong, E. Kifle, X. Mateos, M. Aguilo, F. Díaz, U. Griebner, V. Petrov, G. H. Kim, and F. Rotermund, Opt. Express **27**, 1488 (2019).
13. A. A. Lagatsky, A. Choudhary, P. Kannan, D. P. Shepherd, W. Sibbett, and C. T. Brown, Opt. Express **21**, 19608 (2013).
14. R. Lan, P. Loiko, X. Mateos, Y. Wang, J. Li, Y. Pan, S. Y. Choi, M. H. Kim, F. Rotermund, A. Yasukevich, K. Yumashev, U. Griebner, and V. Petrov, Appl. Opt. **55**, 4877 (2016).
15. P. Loiko, J. M. Serres, X. Mateos, K. Yumashev, A. Yasukevich, V. Petrov, U. Griebner, M. Aguilo, and F. Díaz, Opt. Lett. **41**, 2620 (2016).
16. P. A. Loiko, J. M. Serres, X. Mateos, J. Liu, H. Zhang, A. S. Yasukevich, K. V. Yumashev, V. Petrov, U. Griebner, M. Aguilo, and F. Díaz, Appl. Phys. B **122**, 105 (2016).
17. K. Tian, X. Dou, H. Yi, W. Han, H. Xu, and J. Liu, Laser Phys. **29**, 015805 (2019).
18. K. Tian, Y. H. Li, J. N. Yang, X. D. Dou, H. H. Xu, W. J. Han, and J. H. Liu, Opt. Comm. **436**, 42 (2019).
19. A. Choudhary, S. J. Beecher, S. Dhingra, B. D'Urso, T. L. Parsonage, J. A. Grant-Jacob, P. Hua, J. I. Mackenzie, R. W. Eason, and D. P. Shepherd, Opt. Lett. **40**, 1912 (2015).
20. J. W. Kim, S. Y. Choi, S. Aravazhi, M. Pollnau, U. Griebner, V. Petrov, S. Bae, K. J. Ahn, D. I. Yeom, and F. Rotermund, AIP Advances **5**, 017110 (2015).
21. L. Ma, Y. Tan, S. Wang, S. Akhmadaliev, S. Zhou, H. Yu, H. Zhang, and F. Chen, Journal of Lightwave Technology **35**, 2642 (2017).
22. S. Y. Choi, T. Calmano, F. Rotermund, and C. Kränkel, Opt. Express **26**, 5140 (2018).
23. V. Petrov, M. C. Pujol, X. Mateos, O. Silvestre, S. Rivier, M. Aguilo, R. M. Sole, J. H. Liu, U. Griebner, and F. Díaz, Laser & Photon. Rev. **1**, 179 (2007).
24. J. A. Caird, S. A. Payne, P. R. Staver, A. J. Ramponi, L. L. Chase, and W. F. Krupke, IEEE Journal of Quantum Electronics **24**, 1077 (1988).
25. A. S. Yasukevich, P. Loiko, N. V. Gusakova, J. M. Serres, X. Mateos, K. V. Yumashev, N. V. Kuleshov, V. Petrov, U. Griebner, M. Aguilo, and F. Díaz, Opt. Comm. **389**, 15 (2017).
26. J. Lee, J. Koo, C. Chi, and J. H. Lee, J. Opt. **16**, 085203 (2014).

27. J. Bogusławski, M. Kowalczyk, P. Iwanowski, A. Hruban, R. Diduszko, K. Piotrowski, K. Dybko, T. Wojciechowski, M. Aleszkiewicz, and J. Sotor, Sci. Rep. **7**, 7428 (2017).

References with titles

1. T. M. Fortier, A. Bartels, and S. A. Diddams, "Octave-spanning Ti:sapphire laser with a repetition rate >1 GHz for optical frequency measurements and comparisons," Opt. Lett. **31**, 1011-1013 (2006).
2. Y. N. Billeh, M. Liu, and T. Buma, "Spectroscopic photoacoustic microscopy using a photonic crystal fiber supercontinuum source," Opt. Express **18**, 18519-18524 (2010).
3. R. Aviles-Espinosa, G. Filippidis, C. Hamilton, G. Malcolm, K. J. Weingarten, T. Südmeyer, Y. Barbarin, U. Keller, S. I.C.O Santos, D. Artigas, and P. Loza-Alvarez, "Compact ultrafast semiconductor disk laser: targeting GFP based nonlinear applications in living organisms" Biomed. Opt. Express **2**, 739-747 (2011).
4. M. P. Moreno, and S. S. Vianna, "Femtosecond 1 GHz Ti:sapphire laser as a tool for coherent spectroscopy in atomic vapor," J. Opt. Soc. Am. B **28**, 2066-2069 (2011).
5. S. Pekarek, T. Südmeyer, S. Lecomte, S. Kundermann, J. M. Dudley, and U. Keller, "Self-referenceable frequency comb from a gigahertz diode-pumped solid-state laser," Opt. Express **19**, 16491-16497 (2011).
6. R. R. Gattass, and E. Mazur, "Femtosecond laser micromachining in transparent materials," Nat. Photonics **2**, 219-225 (2008).
7. F. Chen, and J. R. V. de Aldana, "Optical waveguides in crystalline dielectric materials produced by femtosecond-laser machining," Laser Photonics Rev. **8**, 251-275 (2014).
8. H. Yu, X. Chen, H. Zhang, X. Xu, X. Hu, Z. Wang, J. Wang, S. Zhuang, and M. Jiang, "Large energy pulse generation modulated by graphene epitaxially grown on silicon carbide," ACS Nano **4**, 7582-7586 (2010).
9. H. Yu, H. Zhang, Y. Wang, C. Zhao, B. Wang, S. Wen, H. Zhang, and J. Wang, "Topological insulator as an optical modulator for pulsed solid-state lasers," Laser Photon. Rev. **7**, L77-L83 (2013).
10. S. Wang, H. Yu, H. Zhang, A. Wang, M. Zhao, Y. Chen, L. Mei, and J. Wang, "Broadband few-layer MoS_2 saturable absorbers," Adv. Mater. **26**, 3538-3544 (2014).
11. Z. Li, Y. X. Zhang, C. Cheng, H. H. Yu, and F. Chen, "6.5 GHz Q-switched mode-locked waveguide lasers based on two-dimensional materials as saturable absorbers," Opt. Express **26**, 11321-11330 (2018).
12. J. W. Kim, S. Y. Choi, J. E. Bae, M. H. Kim, Y. U. Jeong, E. Kifle, X. Mateos, M. Aguilo, F. Díaz, U. Griebner, V. Petrov, G. H. Kim, and F. Rotermund, "Comparative study of Yb:KYW planar waveguide lasers Q-switched by direct- and evanescent-field interaction with carbon nanotubes," Opt. Express **27**, 1488-1496 (2019).
13. A. A. Lagatsky, A. Choudhary, P. Kannan, D. P. Shepherd, W. Sibbett, and C. T. Brown, "Fundamentally mode-locked, femtosecond waveguide oscillators with multi-gigahertz repetition frequencies up to 15 GHz," Opt. Express **21**, 19608-19614 (2013).
14. R. Lan, P. Loiko, X. Mateos, Y. Wang, J. Li, Y. Pan, S. Y. Choi, M. H. Kim, F. Rotermund, A. Yasukevich, K. Yumashev, U. Griebner, and V. Petrov, "Passive Q-switching of microchip lasers based on Ho:YAG ceramics," Appl. Opt. **55**, 4877-4887 (2016).
15. P. Loiko, J. M. Serres, X. Mateos, K. Yumashev, A. Yasukevich, V. Petrov, U. Griebner, M. Aguilo, and F. Díaz, "Sub-nanosecond Yb:$KLu(WO_4)_2$ microchip laser," Opt. Lett. **41**, 2620-2623 (2016).
16. P. A. Loiko, J. M. Serres, X. Mateos, J. Liu, H. Zhang, A. S. Yasukevich, K. V. Yumashev, V. Petrov, U. Griebner, M. Aguilo, and F. Díaz, "Passive Q-switching of Yb bulk lasers by a graphene saturable absorber," Appl. Phys. B **122**, 105 (2016).
17. K. Tian, X. Dou, H. Yi, W. Han, H. Xu, and J. Liu, "Anomalous passive Q-switching induced by Cr^{4+}:YAG: with pulse repetition rate approaching up to 1 MHz," Laser Phys. **29**, 015805 (2019).
18. K. Tian, Y. H. Li, J. N. Yang, X. D. Dou, H. H. Xu, W. J. Han, and J. H. Liu, "Passive Q-switching of an Yb:$KLu(WO_4)_2$ laser with 2D saturable absorbers of MoS_2 and WS_2: Scaling the output power to 2-W level," Opt. Comm. **436**, 42-46 (2019).
19. A. Choudhary, S. J. Beecher, S. Dhingra, B. D'Urso, T. L. Parsonage, J. A. Grant-Jacob, P. Hua, J. I. Mackenzie, R. W. Eason, and D. P. Shepherd, "456-mW graphene Q-switched Yb:yttria waveguide laser by evanescent-field interaction," Opt. Lett. **40**, 1912-1915 (2015).
20. J. W. Kim, S. Y. Choi, S. Aravazhi, M. Pollnau, U. Griebner, V. Petrov, S. Bae, K. J. Ahn, D. I. Yeom, and F. Rotermund, "Graphene Q-switched Yb:KYW planar waveguide laser," AIP Advances **5**, 017110 (2015).
21. L. Ma, Y. Tan, S. Wang, S. Akhmadaliev, S. Zhou, H. Yu, H. Zhang, and F. Chen, "Continuous-Wave and Q-Switched Yb:YSGG Waveguide Laser," Journal of Lightwave Technology **35**, 2642-2645 (2017).
22. S. Y. Choi, T. Calmano, F. Rotermund, and C. Kränkel, "2-GHz carbon nanotube mode-locked Yb:YAG channel waveguide laser," Opt. Express **26**, 5140-5145 (2018).
23. V. Petrov, M. C. Pujol, X. Mateos, O. Silvestre, S. Rivier, M. Aguilo, R. M. Sole, J. H. Liu, U. Griebner, and F. Díaz, "Growth and properties of $KLu(WO_4)_2$, and novel ytterbium and thulium lasers based on this monoclinic crystalline host," Laser & Photon. Rev. **1**, 179-212 (2007).
24. J. A. Caird, S. A. Payne, P. R. Staver, A. J. Ramponi, L. L. Chase, and W. F. Krupke, "Quantum electronic properties of the $Na_3Ga_2Li_3F_{12}:Cr^{3+}$ Laser," IEEE Journal of Quantum Electronics **24**, 1077-1099 (1988).
25. A. S. Yasukevich, P. Loiko, N. V. Gusakova, J. M. Serres, X. Mateos, K. V. Yumashev, N. V. Kuleshov, V. Petrov, U. Griebner, M. Aguilo, and F. Díaz, "Modelling of graphene Q-switched Tm lasers," Opt. Comm. **389**, 15-22 (2017).
26. J. Lee, J. Koo, C. Chi, and J. H. Lee, "All-fiberized, passively Q-switched 1.06 μm laser using a bulk-structured Bi_2Te_3 topological insulator," J. Opt. **16**, 085203 (2014).
27. J. Bogusławski, M. Kowalczyk, P. Iwanowski, A. Hruban, R. Diduszko, K. Piotrowski, K. Dybko, T. Wojciechowski, M. Aleszkiewicz, and J. Sotor, "Exploiting nonlinear properties of pure and Sn-doped Bi_2Te_2Se for passive Q-switching of all-polarization maintaining ytterbium-and erbium-doped fiber lasers" Sci. Rep. **7**, 7428 (2017).